

Modeling and migration by a new finite difference scheme based on the Galerkin method for irregular grids

Xiang Du and John C. Bancroft

ABSTRACT

Full wave equation 2D modeling and migration using a new finite difference scheme based on the Galerkin method (FDGM) for irregular grids are presented. Since these involve semi-discretization by the finite element method (FEM) in the depth direction with the linear element, spatially irregular grids can be used to compute the wavefield in modeling and reverse-time migration. The mesh can be made locally thin to better represent structural complexity and lower velocity zones, which are treated by a fine grid, while the remaining parts of the models are represented by a coarse grid with equal accuracy. No interpolation is needed between the fine and coarse parts due to the rectangular grid cells. The accuracy of the proposed technique has been tested with a comparison to an analytical solution. The effectiveness of the method is verified by its application to a thin-layer model. At the same time, its efficiency is shown through an impulse and an oblique interface with a variable velocity media.

INTRODUCTION

The design of finite-difference (FD) schemes to handle nonuniform grids is an important topic in seismic modeling and migration. It offers the possibility of a more rational discretization in which the mesh can be made locally thin to better represent structural complexities and low velocity zones, avoiding oversampling in the rest of the model. A simple kind of irregular rectangular mesh may be obtained by variation of the sample interval along the x - and z -axes. Mufti et al. (1996) demonstrated that a variable vertical grid step which adapts to the changes in the velocity with depth can greatly increase the efficiency of the acoustic-wave reversed time migration. In the elastic case, Oprsal and Zahradník (1999) developed a FD scheme to solve the wave equation for displacements in irregular rectangular grids. Sergio (2003) extended the work to apply a fourth-order FD approximation to the complete acoustic wave equation and handle irregular rectangular grids. Pitarka (1999) put forward the velocity-stress formulation for nonuniform rectangular staggered grids. This paper presents a new approach to build irregular grids based on the Galerkin method. Considering that the field seismic data are uniformly recorded along the survey line, and velocities of layers change with the depth, a FD scheme with an irregular grid along the depth direction and a regular grid along the survey line is treated in this work. Following the Galerkin method, we used finite element discretization along the depth direction and the FD method in the spatial domain to solve partial differential equations, which has been clearly addressed by Du and Bancroft (2004). In previous work, we tested the effect of the new method on a regular mesh. Since the FEM discretization along the depth direction is applied, the irregular grid computation along the depth direction will be adopted. As a result, oversampling of large high-velocity areas, typical for fine regular grids, is avoided in this way; it also offers the

possibility of a more rational discretization to make the mesh locally thin to better represent structural complexity and low velocity zone.

The accuracy of the proposed technique was tested by comparing a numerical solution with an analytical solution. The effectiveness of the method is verified by modeling regular meshes and irregular meshes. The efficiency in reverse-time migration is shown by an impulse model migration and an oblique interface with variable velocity media migration.

PRINCIPLE

Consider the hyperbolic model problem, with the 2-D scalar wave equation:

$$\frac{\partial^2 u}{\partial x^2} + \frac{\partial^2 u}{\partial z^2} = \frac{1}{a^2(x, z)} \frac{\partial^2 u}{\partial t^2}, \quad \text{in } \Omega, \quad (1)$$

where $u(x, z, t)$ denotes the wave displacement in the horizontal coordinate x , vertical coordinate z (where the z axis points downward) and time t , respectively, and $a(x, z)$ is the medium velocity.

FEM semi-discretization in the z direction

Semi-discretizing the vertical coordinate (z) in the region of $[0, Z]$, one constructs a finite element function space as

$$u_h(x, z, t) = \sum_{i=1}^N u_i(t, x) N_i(z), \quad (2a)$$

and

$$\frac{\partial}{\partial z} u_h(x, z, t) = \sum_{i=1}^N u_i(t, x) \frac{d}{dz} N_i(z) = \sum_{i=1}^N u_i(t, x) B_i(z), \quad (2b)$$

where N is the nodal number. According to the Galerkin method (Lu and Guan, 1987), one can write the semi-discretized PDEs as:

$$M \frac{\partial^2 u}{\partial t^2} + Ku = H \frac{\partial^2 u}{\partial x^2} \quad (3a)$$

where

$$M = \sum_{n=1}^{N_e} M_e, \quad K = \sum_{n=1}^{N_e} K_e, \quad H = \sum_{n=1}^{N_e} H_e, \quad (3b)$$

$$M_e = \int_e \frac{1}{a(x,z)} N^T N dz, \quad K_e = \int_e B^T B dz, \quad H_e = \int_e N^T N dz. \quad (3c)$$

where e represents the each node, and N_e is the total number of elements. In this paper, the line element is considered for the semi-discretization along the z direction. The linear element length is h and the velocity is a . The interpolation function is $N(z) = (\xi, 1 - \xi)$, with $\xi = \frac{z_{i+1} - z}{h}$ and $h = z_{i+1} - z_i$. The discretization along the z direction by the FEM can be seen from Figure 1. The interpolation functions at each node are shown in Figure 2. From them, we can design the spacing interval according to the complexity of our research model.

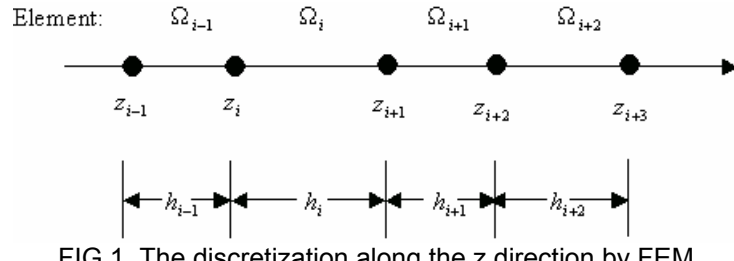


FIG 1. The discretization along the z direction by FEM.

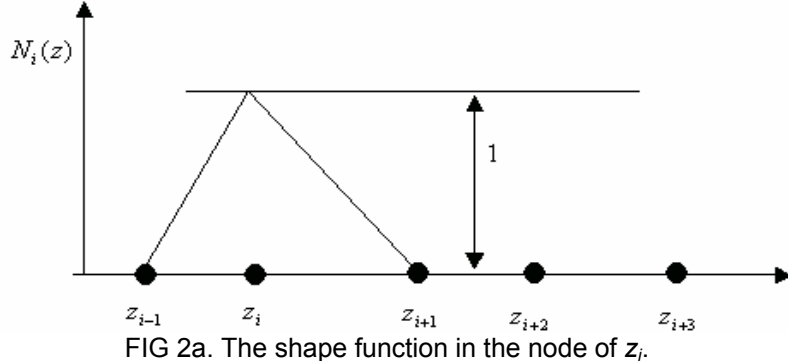


FIG 2a. The shape function in the node of z_i .

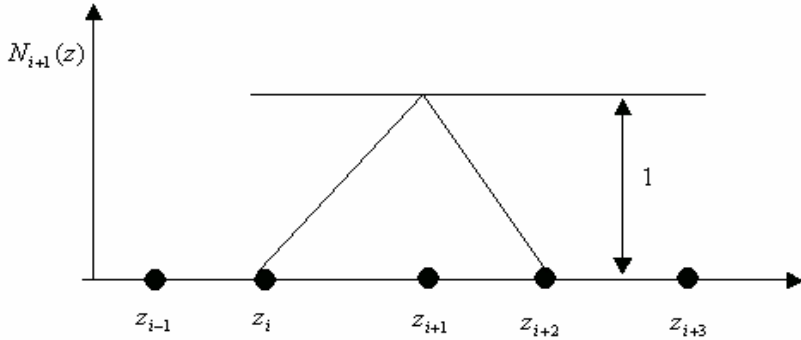


FIG 2b. The shape function in the node of z_{i+1} .

The coefficient matrix of Equation (3a) is

$$M_e = \frac{1}{6a^2} \begin{bmatrix} 2 & 1 \\ 1 & 2 \end{bmatrix}, \quad K_e = \frac{1}{l^2} \begin{bmatrix} 1 & -1 \\ -1 & 1 \end{bmatrix}, \quad H_e = \frac{1}{6} \begin{bmatrix} 2 & 1 \\ 1 & 2 \end{bmatrix}.$$

After all the elements are assembled, we can get the global matrix. Consider the matrix

$$A = \begin{bmatrix} \gamma_1 & \beta_1 & & & & \\ \alpha_2 & \gamma_2 & \beta_2 & & & \\ \alpha_3 & \gamma_3 & \beta_3 & & & \\ & \ddots & \ddots & \ddots & & \\ & & \ddots & \ddots & \ddots & \\ & & & \alpha_{j-1} & \gamma_{j-1} & \beta_{j-1} \\ & & & \alpha_j & \gamma_j & \beta_j \\ & & & \alpha_{j+1} & \gamma_{j+1} & \end{bmatrix},$$

with $\alpha_{j+1} = \beta_j$, which can be used to represent the mass matrix, stiffness matrix and H matrix. We can see that the assembly matrix is tridiagonal and symmetrical. When we assume the discretization has the same space interval,

$$H = \frac{1}{6} \begin{bmatrix} 2 & -1 & & & & & & & \\ 1 & 4 & 1 & & & & & & \\ & 1 & 4 & 1 & & & & & \\ & & 1 & 4 & 1 & & & & \\ & & & 1 & 4 & 1 & & & \\ & & & & 1 & 4 & 1 & & \\ & & & & & 1 & 4 & 1 & \\ & & & & & & 1 & 4 & 1 \\ & & & & & & & 1 & 2 \\ & & & & & & & & 1 \end{bmatrix}, \quad K = \frac{1}{\ell^2} \begin{bmatrix} 1 & -1 & & & & & & & \\ -1 & 2 & -1 & & & & & & \\ & -1 & 2 & -1 & & & & & \\ & & -1 & 2 & +1 & & & & \\ & & & -1 & 2 & -1 & & & \\ & & & & -1 & 2 & -1 & & \\ & & & & & -1 & 2 & +1 & \\ & & & & & & -1 & 2 & -1 \\ & & & & & & & -1 & 1 \end{bmatrix},$$

and M is similar to K , with each element divided by the square of the velocity, which will be used in later numerical tests.

FDM solution of matrix PDEs

A set of indices i, j and n is chosen to establish a discretization model with different grid spacing Δx , Δy and Δt in x, y and t , respectively:

$$\begin{aligned} x &= (i-1)\Delta x & i &= 1, 2, \dots, I \\ y &= (j-1)\Delta y & j &= 1, 2, \dots, J \\ t &= (n-1)\Delta t & n &= 1, 2, \dots, N, \end{aligned}$$

where I, J and N are the number of samples in x, y and t , respectively. One of the explicit schemes, the three-point central scheme, is selected to solve this problem. The difference equation has the form

$$M \frac{1}{\tau^2} (u[i]_j^{n-1} - 2u[i]_j^n + u[i]_j^{n+1}) + Ku[i]_j^n = \frac{H}{12l^2} (u[i-1]_j^{n-1} - 2u[i]_j^n + u[i+1]_j^{n+1}), \quad (4)$$

here $u[i]_j^n$ represents the discrete value of the wavefield at the grid point (i, j) and at time n , τ and l are the time and space steps, assumed constant. When the irregular grids are adopted, and matrices M and H are applied by massed matrices, Equation (4) will become the standard three-point finite difference scheme as following:

$$u[i]_j^{n-1} - 2u[i]_j^n + u[i]_j^{n+1} = \left(\frac{\nu\tau}{h}\right)^2 (u[i-1]_j^n - 2u[i]_j^n + u[i+1]_j^n) + \left(\frac{\nu\tau}{l}\right)^2 (u[i]_{j-1}^n - 2u[i]_j^n + u[i]_{j+1}^n). \quad (5)$$

Therefore, the presented scheme has much wider application for regular grids but also the irregular grids. As for the stability conditions of this method, they have been discussed in previous work by Du and Bancroft (2004), which show that it has much more relaxed conditions than traditional finite difference scheme with the same accuracy by Wu, et al.(1996).

NUMERICAL EXAMPLES

In order to validate the algorithms of FDGM for irregular grids, four cases are chosen for modeling and migration. The numerical solution of using irregular grids for a half-plane problem is compared with the corresponding analytical solution. We also present an example of efficiently modeling wave propagation in a thin-layer model. For migration, an impulse model with constant velocity and an oblique interface model with variable velocities are chosen to show the computational efficiency of the irregular grids.

Case I: Comparison between the numerical solution with the irregular grids and analytical solution of the half-plane problem

The half-plane problem is a particular case of the infinite-wedge problem. As underlined by Wait (1959), the solution can be found by image theory. A source S inside the medium induces one virtual image source. The image S' is symmetric with respect to the real source. For a point source $S(x_s, z_s)$ with a time function $f(t_s)$, one can write the solution at the point $M(x, z)$ as

$$\begin{aligned} G(x, z, t, x_s, z_s, t_s) * f(t_s) & \quad \text{incident wave,} \\ -G(x, z, t, x_s, -z_s, t_s) * f(t_s) & \quad \text{boundary reflection wave,} \end{aligned} \quad (6)$$

where $G(x, z, t, x_s, z_s, t_s)$ is the Green's function for the infinite medium given as $H(t - r/c) / \sqrt{t^2 - r^2/c^2}$ with $r^2 = (x - x_s)^2 + (y - y_s)^2$.

Table 1. Half-plane parameters.

Physical parameters	
Velocity	3000 m/s
Source and Observer Position	$f_{main} = 50\text{Hz}$; source position: (250, 250); observer position: (150, 150).
Other parameters	$dx = 5\text{m}$, $dz = 4\text{ m(odd lines)}/6\text{ m(even lines)}$, $dt = 1.25\text{E-3s}$, grid of 300×300 points

Table 1 gives the physical parameters of the half-plane problem. Considering the usual rule of using at least ten points for the shortest wavelength of the source in this FD scheme, the grid interval along the depth alternately changes between 4 meter and 6 meter. The seismogram at a given point (Table 1) shows more quantitatively the accuracy of the numerical solution by comparison with the analytical solution (Figure 3). They are accurately matched except some difference in the amplitude.

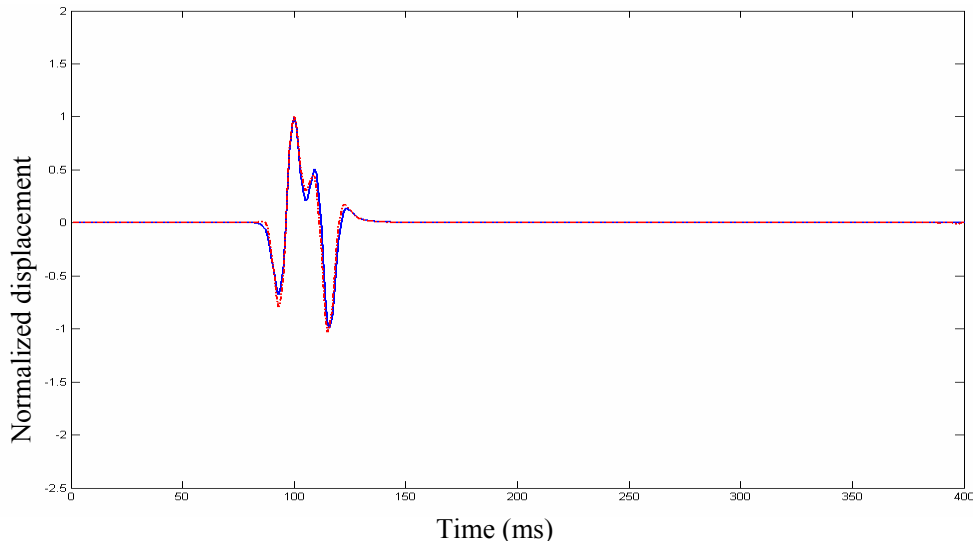


FIG 3. Seismogram at the given observer position (Table 1). The solid blue line is the analytical solution, the dashed green line is the numerical solution by FDGM with irregular grids.

Case II: Comparison between the numerical solution with regular grid and irregular grid for thin-layer model

The accuracy of the proposed FD technique has been verified for the homogeneous region shown as Case I. Now we apply it to effectively model wave propagation in a thin-layer model. Tests include both regular and irregular grid calculations. The size of the model is $1500\text{ m} \times 1800\text{ m}$. A thin-layer with 12 m thickness is imbedded in the model. The purpose is to see if the effects of the thin-layer with lower velocity can be observed in snapshots of the wavefield. The Ricker wavelet with 50 Hz is selected as the source centered in the horizontal direction and located 600 m below the top. The velocity of the thin layer is 2000 m/s, while the background velocity 4000 m/s, which are shown in Figure 4. The horizontal spacing is 5 m. For the regular grid calculation, the grid step of

vertical spacing used is 6 m. In the irregular mesh, the thin grid is used only in the region of lower velocity, which is shown in the Figure 5, and the grid interval is 3 m. Other grid spacing along the depth direction is 7 m. So, the regular grid requires a total of 300×300 points, where the irregular one needs 300×260 points, which saves almost 24% fewer points compared to the regular case. The same time step ($\Delta t = 0.001$ s) is used in both cases.

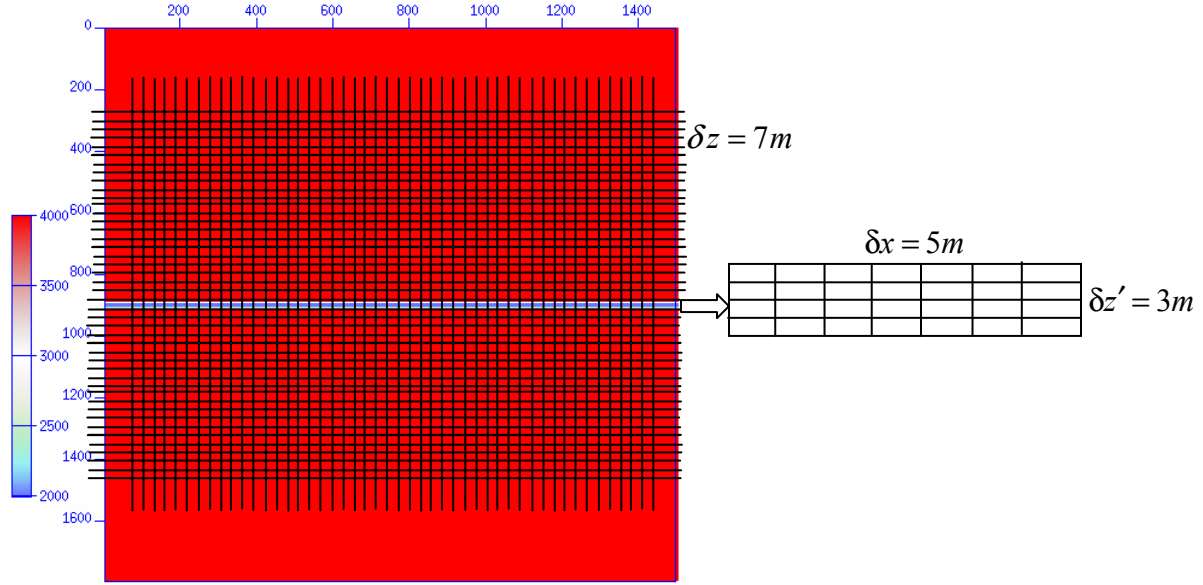


FIG 4. The velocity model and the grids partition.

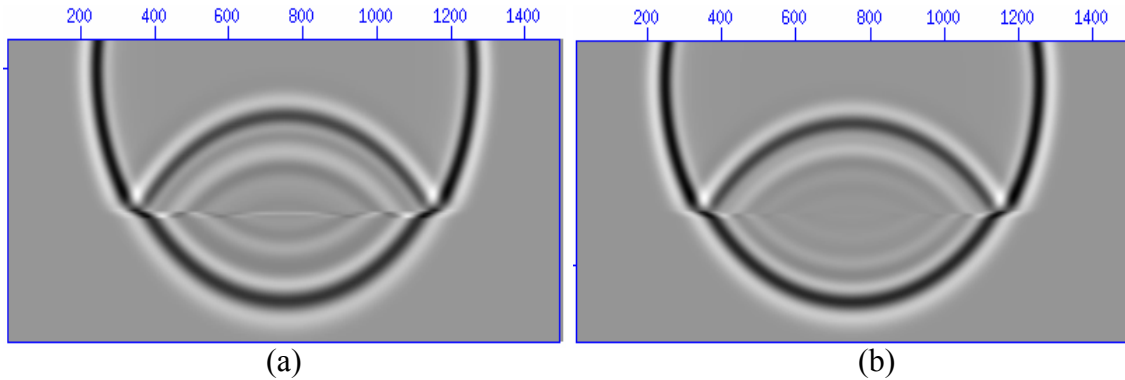


FIG 5(a) Snapshot of the wavefield ($t = 0.15$ s) with regular girds, and (b) snapshot of the wavefield ($t = 0.15$ s) with irregular grids.

In order to show the result with irregular grids, we apply the cubic spline interpolation function to interpolate the one with regular grids. As for the thin-layer model, we focus our attention on the wavefield character when the wave propagates into the thin-layer. Figure 5 shows a wavefield snapshot at time 0.15 s. Reflections and transmissions from the thin lower-velocity layer can be seen. From Figure 5a, there is obvious frequency dispersion in the region of the thin-layer because a coarse grid is used in the area, while the continuity of the wavefield in the thin-layer is well described in Figure 5b.

Case III: Impulses and flat events migration with irregular grids

To test the migration accuracy of FDGM with irregular grids, an impulses and flat events model is designed. The poststack profile of a constant-velocity medium ($a=3000$ m/s) is shown as Figure 6. The Ricker wavelet with zero-phase is used, with a main frequency of 50 Hz and sampling interval of 1 ms. The first three impulses are respectively located at $x=260$ m, 262.5 m, 265 m (lateral) and $t=0.1$ s (time). In addition, the amplitude of the first three impulses is 0.25, 0.75 and 0.25 from the left to the right. The fourth impulse is located at $x=261$ m and $t=0.2$ s. The remaining feature is the flat event that is present in all the traces at $t=0.3$ s.

In reverse-time migration, the spacing interval along the x direction is 2.5 m. considering the frequency dispersion and the dipping angle image, the depth interval above 300 m is 2.5 m, while the one of the left 300 m is 4 m. The migration result is shown in Figure 7. We can see that the FDGM with irregular grids well demonstrates the imaging ability for a dipping angle and flat events with high accuracy and efficiency.

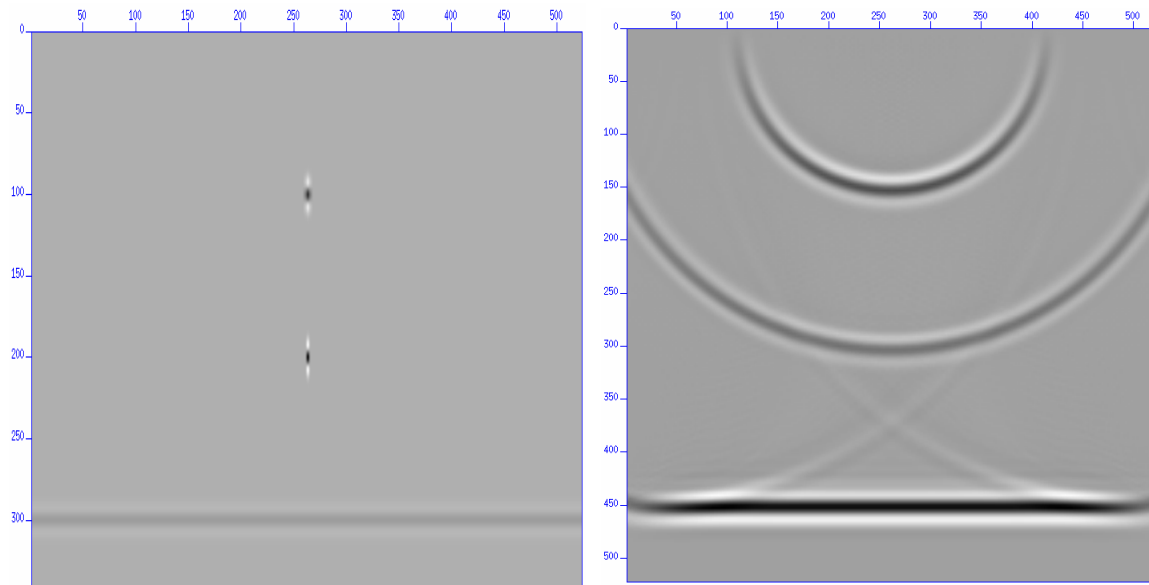


FIG 6. Impulses and flat events seismic sections.

FIG 7. The migrated result by FDGM.

Case IV: Steep oblique interfaces migration with variable velocities

The model for this section is shown in Figure 8. The velocity of the model increases both laterally and with depth direction. The velocity at the top left corner is 3600 m/s, and the at the bottom right it is 4600 m/s. There are four reflection interfaces with a dip of 0°, 23°, 45°, and 70°. The seismogram is computed by the FDM module of the SU Software Kit, and is displayed in Figure 9. From it, one can see that there is much diffraction energy from the edges of the reflectors.

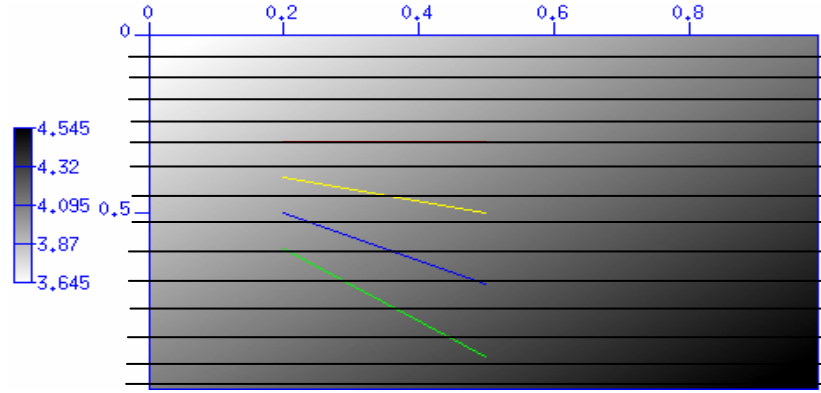


FIG 8. The steep oblique model with variable velocities.

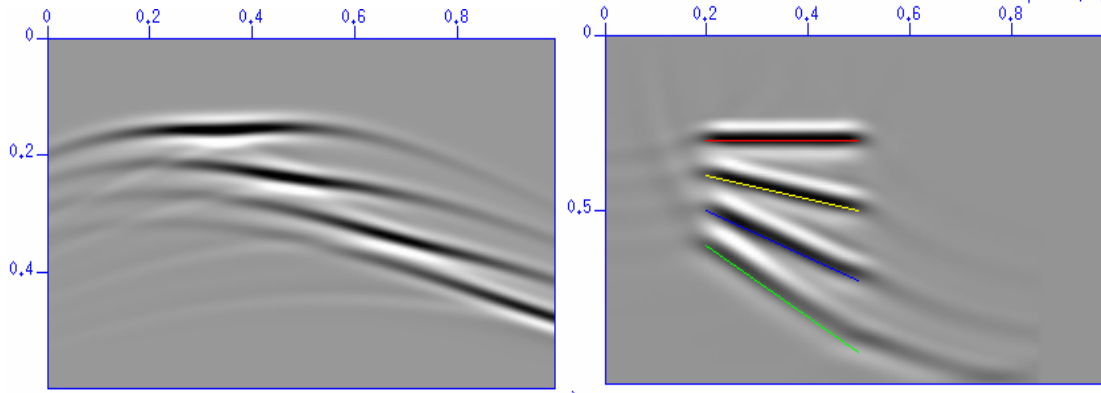
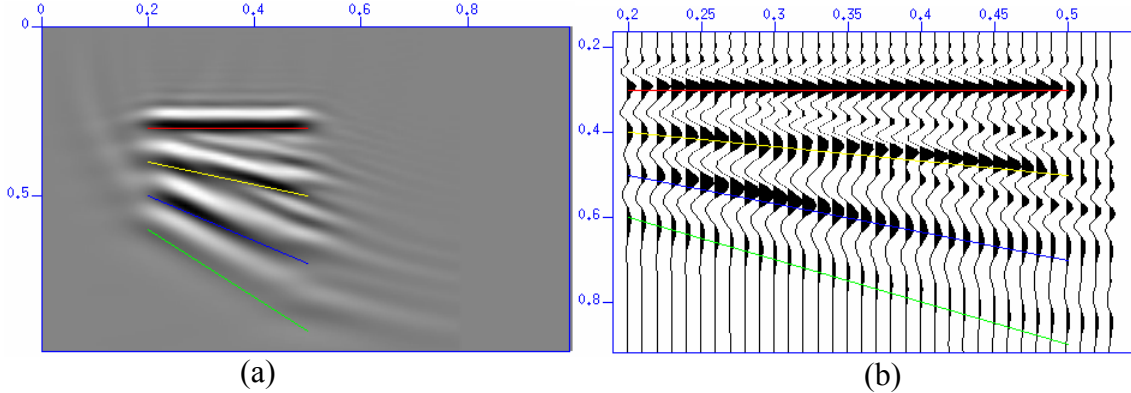


FIG. 9. Seismogram generated by FDM.

FIG. 10. Reverse-time migration result($\Delta z=0.04\text{m}$).FIG 11(a). A grayscale display of the reverse-time migration result($\Delta z=0.15\text{ m}$), and (b) a wiggle trace display.

The parameters for reverse-time migration start with a grid interval of 10 m and increase by 0.04 m on each grid to a final interval of 20 m. The velocity increases in the spatial direction from 3600 to 4500. The regular grid with 10 m spacing requires a total of 100×100 , while the irregular grid requires only 100×85 , which saves some calculations. The grids partition is also shown in Figure 8. Figure 10 is the reverse-time migration result, which correctly migrated the poststack seismic section to the right oblique interface. Since there is truncation in the seismogram, we can still see some

diffraction energy, which doesn't affect the migration result. When the grid spacing increases with 0.15m, the irregular one requires only 100×63 , which saves a lot of memory and calculations. The migration results are shown in Figure 11. From Figure 11a, we know there is obvious frequency dispersion problem, but from Figure 11b, there is still a good match between the events and the real interfaces.

CONCLUSIONS

This paper presents a FDGM approximation for the full acoustic wave equation which is able to handle nonuniform rectangular grids. The new scheme has achieved the same accuracy of a thin regular-grid calculation while reducing the computational cost in modeling and reverse-time migration. As numerical examples, it is encouraging that the result is accurate and effective enough for the simulation and migration of a complex wavefield. It is therefore a useful and promising numerical method. Only the linear element was applied along the depth direction, but extension to a quadratic element is straightforward, which gives a higher order accuracy. It is possible that a FDGM scheme for the elastic case may also be designed using the same approach. At the same time, we can construct the irregular grids FD calculation for both the horizontal direction and vertical direction by a two-dimensional interpolation function.

ACKNOWLEDGEMENTS

We should sincerely express gratitude to Larry Lines, Edward S. Krebes and Chuck Ursenbach for helpful discussions. We should also express thanks for sponsors of the CREWES project.

REFERENCES

- Du, X., and Bancroft, J., 2004, 2-D wave equation modeling and migration by a new finite difference scheme based on Galerkin method, 74th Ann. Internet Mtg., Soc. Expl. Geophys., U.S.A
- Lu, J. and Guan, Z., 1987, Numerical method of partial differential equations (In Chinese), Beijing: Tsinghua University Press.
- Mufti, I. R., Pita, J. A., and Huntley, R.W., 1996, Finite-difference depth migration of extrapolation scale 3-D seismic data: *Geophysics*, **61**, 776–794.
- Opsal, I., and Zahradnik, J., 1999, Elastic finite-difference method for irregular grids: *Geophysics*, **64**, 240–250.
- Pitarka, A., 1999, 3D elastic finite-difference modeling of seismic motion using staggered grids with nonuniform spacing: *Bull. Seis. Soc. Am.*, **89**, 54–68.
- Sergio, A., 2003, A fourth-order finite-difference method for the acoustic wave equation on irregular grids: *Geophysics*, **68**, 672–676.
- Wait, J. R., 1959, Electro-magnetic radiation from cylindrical structure: Pergamon Press Inc.
- Wu, W., Lines, L. R., and Lu, H., 1996, Analysis of higher-order finite difference schemes in 3-D reverse-time migration: *geophysics*, **61**, 845–856.